Scientia Iranica F (2020) 27(6), 3454–3466

Sharif University of Technology
Scientia Iranica
Transactions F: Nanotechnology
http://scientiairanica.sharif.edu

Research Note

Computational analysis of unsteady and steady magnetohydrodynamic radiating nanofluid flows past a slippery stretching sheet immersed in a permeable medium

M.A. Farooq[a,*], A. Salahuddin[a], M. Razzaq[b], S. Hussain[c], and A. Mushtaq[d]

a. *Department of Mathematics, School of Natural Sciences (SNS), National University of Sciences and Technology (NUST), Sector H-12, 44000, Islamabad, Pakistan.*
b. *Department of Mathematics, Lahore University of Management Sciences (LUMS), 54792, Lahore, Pakistan.*
c. *Chah Ranjhay Wala, Post Office Bangla Morr, Tehsil Shujaabad, Multan, Pakistan.*
d. *Seksjon for Matematikk, Nord Universitet, 8026 Bodφ, Norway.*

Received 1 March 2019; received in revised form 26 February 2020; accepted 8 June 2020

KEYWORDS
Magnetohydrodynamic (MHD);
Slippery sheet;
Porous medium;
Nanofluid;
Node-centered finite volume method.

Abstract. This paper discusses unsteady/steady radiating magnetohydrodynamic (MHD) nanofluid flow over a slippery stretching sheet. Introducing similarity variables reduced the Partial Differential Equations (PDEs) to a new set of PDEs in which the solution was a function of two independent variables. For time integration, first-order explicit Euler method was performed and spatial derivatives were approximated by the finite differences. The steady flow solution was computed by the built-in *bvp4c* solver in MATLAB. The flow regime was controlled by a number of thermophysical parameters, namely thermal Grashof number (Gr), Lewis number (Le), Eckert number (Ec), Brownian motion (Nb), thermophoresis (Nt), heat source or sink (S), Prandtl number (Pr), magnetic field (M), and Darcy number (Da). The findings were evaluated by graphs and tables for velocity, temperature, and concentration profiles as well as the skin friction coefficient, the local Nusselt number, and the local Sherwood number. The results converged in the grid convergence test. In the unsteady flow, the temperature of the nanofluid was higher near the surface without the thermophoresis parameter (Nt) and significantly decreased in the presence of Nt. Moreover, concentration boundary layer thickness decreased with an increase in the Darcy number (Da).

1. Introduction

Today, more than ever, cooling of devices is one of the most pressing needs in many industrial technologies because of their ever-increasing heat generation rates at both micro (e.g., computer chips) and macro (e.g., car engines) levels. An abundance of cases exist in which the operational cost of the end product and mechanical work is highly dependent on the cooling rate of a process. For instance, the process of metal extraction from ores necessitates accurate calculation of heat transfer rate [1]. Other examples of the application of heat transfer rate can be found in electronic devices, vehicle cooling, heat exchangers, and nuclear reactors [2].

*. *Corresponding author. Tel.: +92-51-9085-5594*
E-mail addresses: asif.farooq@sns.nust.edu.pk (M.A. Farooq); aishasalahuddin3@gmail.com(A. Salahuddin); mudassar.razzaq@lums.edu.pk (M. Razzaq); rana-sabir@hotmail.com (S. Hussain); asif.mushtaq@nord.no (A. Mushtaq)

doi: 10.24200/sci.2020.53055.3039

Thermal conductivity of fluids can be increased by adding nanoparticles 100 nm in size to the base fluid (which is usually water). A colloidal suspension containing a mixture of nanoparticles and water is generally identified as a nanofluid, a term coined by Choi and Eastman [3]. Nanofluids have gained a prime importance in all walks of life, e.g., vehicle coolants, brake fluids, domestic refrigerators, etc. [4–8]. Some of their usages are in electronics (heat transfer), agriculture (energy harvesting systems), medicine (anti-infection therapy, hyperthermia), etc. [9–11]. A very comprehensive review of nanofluids has been provided in [8]. Buongiorno [12] studied various slip mechanisms between nanoparticles and the base fluid. Seven slip mechanisms, namely inertia, Brownian diffusion, thermophoresis, diffusiophoresis, magnus effect, fluid drainage, and gravity, went under their investigation and Brownian diffusion and thermophoresis were found as the important slip mechanisms in the absence of turbulent effects. They also observed enhancement in heat transfer under convective conditions. In another study, Das et al. [13] examined boundary layer flow of nanofluid over a stretching sheet in the presence of thermal radiation with unsteady stream condition. They made enquiries into the effects of Brownian motion and thermophoresis. An interesting study of time-dependent tangent hyperbolic nanofluid flow over a wedge has been presented in [14]. In this study, the shooting technique was adopted for two types of wedges, namely static and stretching and an enhanced temperature profile was seen against different physical properties. A revised approach to the solar energy aspect of time-dependent magnetohydrodynamic (MHD) cross nanofluid is discussed in [15]. The problem was treated numerically and the solution was achieved by applying the shooting technique. It was indicated that the magnetic parameter influenced the wall shear stress. For further information on this topic, the reader is referred to [16–18].

Many researchers have recently paid attention to the study flow and heat transfer in electrically conducting continuous fluid under the influence of an applied magnetic field considering the fact that it provides a substantially wide range of applications to aerodynamics and many engineering problems such as MHD generators, MHD pumps, plasma, jet printer, nuclear reactors, and liquid metals. Rossow [19] was probably the first researcher who studied the hydrodynamic behavior of the boundary layer on a semi-infinite flat plate in the presence of a uniform magnetic field. Thermal radiation effect on MHD flow was discussed in [20]. Also, slip MHD flow was discussed in [21].

Makinde et al. [22] examined the variable viscosity effect of nanofluid on a radially stretching surface with radiative heat. Nield and Kuznetsov [23] presented convective boundary layer nanofluid flow in a porous medium. Hayat et al. [24] discussed the simultaneous effect of internal heat generation in Jeffery fluid on a nonlinear stretching surface with variable thickness. Analysis of unsteady flow is also important in aerodynamics, nuclear plants, and space vehicles. Makinde et al. [25] considered multiple factors to present a finite difference solution for unsteady flow over a slippery stretching sheet in a porous medium. Malik et al. [26] discussed boundary layer flow of Casson nanofluid over a vertically exponentially stretching cylinder. Jusoh et al. [27] found a dual solution for MHD 3D nanofluid flow over a permeable stretching and shrinking sheet surface with velocity slip and thermal radiation. Reddy et al. [28] discussed variable fluid properties of slip flow of copper (Cu) based nanofluid over a stretching sheet with convective boundary conditions. Hakeem et al. [29] discussed the partial slip effect of flow over a porous sheet considering thermal radiation and wall mass transfer. Cortell [30] discussed the heat transfer flow in a porous medium with internal heat generation and absorption. Cai et al. [31] considered the unsteady convective flow over a vertically stretching surface. For some more information on partial slip, cf. [32–36].

Numerical methods have become widespread procedures to solve coupled differential equations. Instances of such methods are Finite Difference Method (FDM), Finite Volume Method (FVM), Finite Element Method (FEM), spectral methods, variational iteration method, shooting methods, *bvp4c*, etc. The variables in FDM, FVM, and FEM are defined on nodes, cells, and elements, respectively. Owing to its simplicity and easy implementation, the FDM is preferred to FVM and FEM in solving Partial Differential Equations (PDEs) for fluid flow [37,38]. Sheikholeslami [39] presented the Control Volume Finite Element Method (CVFEM) to solve nanofluid flow inside a porous medium considering Brownian motion. Recently, Reza-E-Rabbi et al. [40] applied explicit finite difference scheme to an unsteady chemically reacting fluid flow over a stretching sheet with Brownian and thermophoresis effects. Makinde et al. [25] also employed the explicit FDM for an unsteady flow. For the system of coupled Ordinary Differential Equations (ODEs), the superior choice among numerical methods is the recently introduced highly accurate collocation solver *bvp4c* written in MATLAB [41].

The general structure of the paper is as follows. Section 2 gives the definition of the physical problem in mathematical terms. Section 3 provides discretization of PDEs for both the spatial and temporal variables. Section 4 presents a steady flow analysis. The findings are discussed in Section 5. Conclusions are drawn in Section 6 at the end.

2. Mathematical formulation

We assume two-dimensional, unsteady, incompressible, laminar, MHD boundary layer flow of an electrically conducting nanofluid over a slippery stretching sheet submerged in a porous medium. The geometry of the problem is shown in Figure 1, in which the x-axis is taken along the sheet and y-axis is normal to it.

Under the above-mentioned assumptions, the governing equations consisting of continuity, momentum, energy, and concentration are construed in the following form using the Buongiorno model [12,25]:

$$\partial_x(u) + \partial_y(v) = 0, \tag{1}$$

$$u_t + uu_x + vu_y = \nu u_{yy} - \frac{\sigma B_o^2 u}{\rho} - \frac{\nu u}{K} + g\beta(T - T_\infty), \tag{2}$$

$$T_t + uT_x + vT_y = \frac{1}{\rho C_p}\partial_y(kT_y) + \frac{\nu}{C_p}(u_y)^2 + \frac{\sigma B_o^2 u^2}{\rho C_p} + \frac{\nu u^2}{C_p K} - \frac{1}{\rho C_p} q_{ry} + \frac{Q(T - T_\infty)}{\rho C_p} + \tau\left[D_B(C_y T_y) + \frac{D_T}{T_\infty}(T_y)^2\right], \tag{3}$$

$$C_t + uC_x + vC_y = D_B(C_{yy}) + \frac{D_T}{T_\infty}(T_{yy}), \tag{4}$$

where (u, v) are the velocity components in the x and y directions. μ is the coefficient of viscosity, ρ is the density of the fluid, σ is electrical conductivity of the fluid, T is fluid temperature, K is permeability of the porous medium, β is the thermal expansion coefficient, k is thermal conductivity, C_p is the specific heat capacity, q_r is radiative heat flux, Q is the heat source coefficient, C is concentration, $\tau = (\rho C)_p/(\rho C)_f$ with $(\rho C)_p$ and $(\rho C)_f$ respectively being heat capacities of nanofluid and base fluid respectively, C_p is the specific heat at constant pressure, D_B and D_T are Brownian and thermophoretic diffusion coefficients, T_∞ is the ambient fluid temperature, and C_∞ is the ambient fluid concentration.

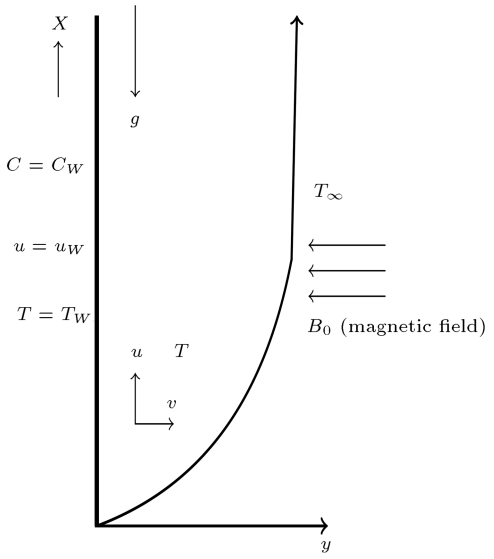

Figure 1. Flow pattern of a slippery stretching sheet.

2.1. Boundary conditions

The incremental boundary conditions are given as:

$$u(x, y, 0) = 0, \quad v(x, y, 0) = 0, \quad T(x, y, 0) = T_\infty, \quad C(x, y, 0) = C_\infty, \tag{5}$$

$$u(x, 0, t) = U_w + \frac{\mu}{L}u_y, \quad v(x, 0, t) = 0, \quad T(x, 0, t) = T_w, \quad C(x, 0, t) = C_w, \tag{6}$$

$$u \to 0, \quad T \to T_\infty, \quad C \to C_\infty \quad \text{as} \quad y \to \infty,$$

where $U_w = ax$ is the stretching velocity, $T_w = T_\infty + bx$ is the variable temperature of sheet with T_∞ being a free stream constant, and $C_w = C_\infty + bx$ is the variable concentration of nanofluid on the sheet with C_∞ being a constant.

2.2. Solution method

The following similarity parameters are introduced to get the non-dimensionalized form of the momentum, energy, and concentration equations as well as the boundary conditions:

$$\eta = \sqrt{\frac{a}{\nu}}y, \quad \psi(\eta) = \sqrt{a\nu}xf(\eta), \quad \tau = at,$$

$$u = ax\frac{\partial f}{\partial \eta}, \quad v = -\sqrt{a\nu}f(\eta),$$

$$\theta(\eta) = \frac{T - T_\infty}{T_w - T_\infty}, \quad \phi(\eta) = \frac{C - C_\infty}{C_w - C_\infty},$$

where η is the similarity variable; τ is the non-dimensional time; and $\psi(\eta)$, $\theta(\eta)$, and $\phi(\eta)$ are dimensionless stream, temperature, and concentration functions, respectively. By employing the above similarity variables, one can reduce Eqs. (2)–(4) into the following nonlinear differential equations

$$\frac{\partial^2 f}{\partial \eta \partial \tau} - f\frac{\partial^2 f}{\partial \eta^2} - \frac{\partial^3 f}{\partial \eta^3} - \left(\frac{\partial f}{\partial \eta}\right)^2 + \left(M + \frac{1}{\mathrm{Da}}\right)\frac{\partial f}{\partial \eta} - \mathrm{Gr}\theta = 0, \tag{7}$$

$$\mathrm{Pr}\frac{\partial \theta}{\partial \tau} + \mathrm{Pr}\left(\theta\frac{\partial f}{\partial \eta} - f\frac{\partial \theta}{\partial \eta}\right) - (1 + Nr)\frac{\partial^2 \theta}{\partial \eta^2} - \mathrm{EcPr}\left(\frac{\partial^2 f}{\partial \eta^2}\right)^2 - \mathrm{EcPr}\left(M + \frac{1}{\mathrm{Da}}\right)\left(\frac{\partial f}{\partial \eta}\right)^2 - \mathrm{Pr}S\theta - \mathrm{Pr}Nb\frac{\partial \theta}{\partial \eta}\frac{\partial \phi}{\partial \eta} - Nt\mathrm{Pr}\left(\frac{\partial \theta}{\partial \eta}\right)^2 = 0, \tag{8}$$

$$\mathrm{Le}\frac{\partial\phi}{\partial\tau}+\mathrm{Le}\Big(\phi\frac{\partial f}{\partial\eta}-f\frac{\partial\phi}{\partial\eta}\Big)-\frac{\partial^2\phi}{\partial\eta^2}-\frac{Nt}{Nb}\frac{\partial^2\theta}{\partial\eta^2}=0, \quad (9)$$

where M, Pr, Nt, Nb, Da, Gr, Ec, S, and Le are the magnetic parameter, Prandtl number, thermophoresis parameter, Brownian parameter, Darcy number, thermal Grashof number, Eckert number, heat source, and Lewis number, respectively. These parameters are defined as [25]:

$$\mathrm{Pr}=\frac{\mu C_p}{k},\quad M=\frac{\sigma B^2}{\rho a},\quad Nt=\frac{\tau D_T(T_w-T_\infty)}{\nu T_\infty},$$

$$Nb=\frac{\tau D_B(C_w-C_\infty)}{\nu},\quad \mathrm{Le}=\frac{\nu}{D_B},\quad \mathrm{Gr}=\frac{\beta g b}{a^2},$$

$$\mathrm{Da}=\frac{Ka}{\nu},\quad \mathrm{Ec}=\frac{au_w}{bC_p},\quad S=\frac{Q}{a\rho C_p}.$$

After transformation, the boundary conditions (5) and (6) take the following forms:

$$\frac{\partial f}{\partial\eta}(\eta,0)=0,\quad f(\eta,0)=0,\quad \theta(\eta,0)=0,$$

$$\phi(\eta,0)=0, \quad (10)$$

$$\frac{\partial f}{\partial\eta}(0,\tau)=1+\lambda\frac{\partial^2 f}{\partial\eta^2}(0,\tau),\quad f(0,\tau)=0,$$

$$\theta(0,\tau)=1,\quad \phi(0,\tau)=1, \quad (11)$$

$$\frac{\partial f}{\partial\eta}(\infty,\tau)=0,\quad \theta(\infty,\tau)=0,\quad \phi(\infty,\tau)=0. \quad (12)$$

The skin friction coefficient C_f is given by [25]:

$$C_f=\frac{\tau_w}{\rho u_w^2},\ \text{where}\ \ u_w=-\frac{\partial u}{\partial y}. \quad (13)$$

The local Nusselt number Nu_x is [25]:

$$\mathrm{Nu}_x=\frac{xq_w}{k(T_w-T_\infty)},\ \text{where:}$$

$$q_w=-k\Big(1+\frac{16\sigma^* T_\infty^3}{3k^* k}\Big)\frac{\partial f}{\partial y}, \quad (14)$$

and the local Sherwood number Sh_x is given by:

$$\mathrm{Sh}_x=\frac{xj_w}{k(C_w-C_\infty)},\text{where}\ \ j_w=-D\frac{\partial C}{\partial y}|_{y=0}. \quad (15)$$

After using the similarity transformations, Eqs. (13), (14), and (15) become:

$$\sqrt{\mathrm{Re}_x}C_f=\frac{\partial^2 f}{\partial\eta^2}(0,\tau),$$

$$\frac{\mathrm{Nu}_x}{\sqrt{\mathrm{Re}_x}}=-(1+Nr)\frac{\partial\theta}{\partial\eta}(0,\tau),$$

$$\frac{\mathrm{Sh}_x}{\sqrt{\mathrm{Re}_x}}=-\frac{\partial\phi}{\partial\eta}(0,\tau).$$

Here, $\mathrm{Re}_x=Ux/\nu$ is a local Reynolds number .

3. Unsteady flow analysis

3.1. Spatial and temporal discretization

We assume a domain $[0\quad \eta_\infty]\times[0\quad \tau_{end}]$ and $N+1$ grid points in η-direction with equidistant grid spacing $\Delta\eta=\frac{\eta_\infty}{N}$ and take τ_{end} as the end time with time step $\Delta\tau=\frac{\tau_{end}}{n_{end}}$. The coordinates of the grid points (i,n) are (η_i,τ_n) where $\eta_i=i\Delta\eta, i=0,1,...,N$ and $\tau_n=n\Delta t, n=0,1,2,....$ The finite difference stencil is shown in Figure 2. For discretization in η-direction we apply backward finite difference approximation to the first-order derivatives and central difference approximations to the second-order derivative. For time integration, we use explicit Euler method. For convenience, in order to implement FDM in MATLAB, we reduce the order of the momentum equation to convert it into a second-order PDE. The order of unsteady temperature and concentration equations is not reduced since it is already determined in the second order. All the finite difference approximations of all derivatives are given below. Now, we explain the procedure for reducing the order of the unsteady momentum equation. Defining $\frac{\partial f}{\partial\eta}=F$, Eqs. (7), (8), and (9), take the following form:

$$\frac{\partial F}{\partial\tau}-f\frac{\partial F}{\partial\eta}-\frac{\partial^2 F}{\partial\eta^2}+(F)^2+(M+\frac{1}{\mathrm{Da}})F$$
$$-\mathrm{Gr}\theta=0, \quad (16)$$

$$\mathrm{Pr}\frac{\partial\theta}{\partial\tau}+\mathrm{Pr}\Big(\theta F-f\frac{\partial\theta}{\partial\eta}\Big)-(1+Nr)\frac{\partial^2\theta}{\partial\eta^2}$$
$$-\mathrm{EcPr}\Big(\frac{\partial F}{\partial\eta}\Big)^2-\mathrm{EcPr}\Big(M+\frac{1}{\mathrm{Da}}\Big)(F)^2$$

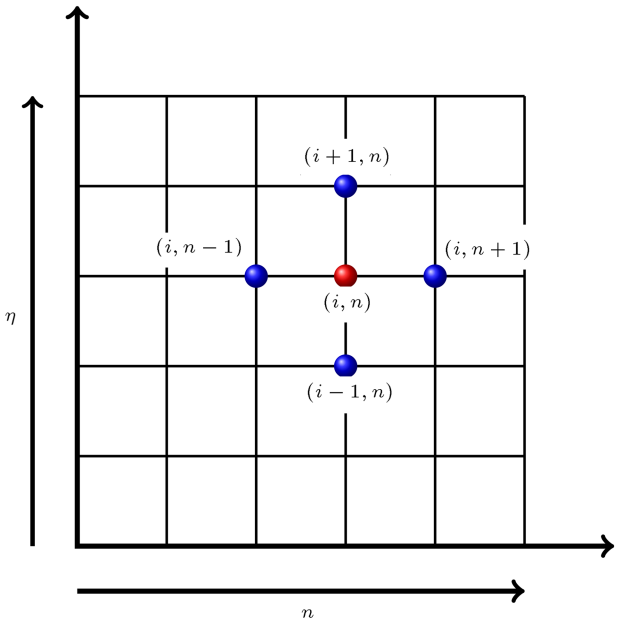

Figure 2. Finite difference grid.

$$-\mathrm{Pr}S\theta-\mathrm{Pr}Nb\frac{\partial\theta}{\partial\eta}\frac{\partial\phi}{\partial\eta}-Nt\mathrm{Pr}\Big(\frac{\partial\theta}{\partial\eta}\Big)^2=0, \quad (17)$$

$$\mathrm{Le}\frac{\partial\phi}{\partial\tau}+\mathrm{Le}\Big(\phi F-f\frac{\partial\phi}{\partial\eta}\Big)-\frac{\partial^2\phi}{\partial\eta^2}-\frac{Nt}{Nb}\frac{\partial^2\theta}{\partial\eta^2}=0. \quad (18)$$

The order of associated boundary conditions (10), (11), and (12) is reduced as:

$$F(\eta,0)=0, \quad f(\eta,0)=0, \quad \theta(\eta,0)=0,$$
$$\phi(\eta,0)=0, \quad (19)$$

$$F(0,\tau)=1+\lambda\frac{\partial F}{\partial\eta}(0,\tau), \quad f(0,\tau)=0,$$
$$\theta(0,\tau)=1, \quad \phi(0,\tau)=1, \quad (20)$$

$$F(\infty,\tau)=0, \quad \theta(\infty,\tau)=0, \quad \phi(\infty,\tau)=0. \quad (21)$$

To solve the above system of equations along with boundary conditions, we approximate the derivatives in the PDEs by linear combinations of function values at the grid points using the FDM. All the finite difference approximations for all orders are given by:

$$\Big(\frac{\partial F}{\partial\eta}\Big)_{(i,n)}=\frac{F_{i+1}^n-F_i^n}{\Delta\eta},$$

$$\Big(\frac{\partial^2 F}{\partial\eta^2}\Big)_{(i,n)}=\frac{F_{i+1}^n-2F_i^n+F_{i-1}^n}{(\Delta\eta)^2},$$

$$\Big(\frac{\partial F}{\partial\tau}\Big)_{(i,n)}=\frac{F_i^{n+1}-F_i^n}{\Delta\tau},$$

$$\Big(\frac{\partial\theta}{\partial\eta}\Big)_{(i,n)}=\frac{\theta_{i+1}^n-\theta_i^n}{\Delta\eta},$$

$$\Big(\frac{\partial^2\theta}{\partial\eta^2}\Big)_{(i,n)}=\frac{\theta_{i+1}^n-2\theta_i^n+\theta_{i-1}^n}{(\Delta\eta)^2},$$

$$\Big(\frac{\partial\theta}{\partial\tau}\Big)_{(i,n)}=\frac{\theta_i^{n+1}-\theta_i^n}{\Delta\tau}$$

$$\Big(\frac{\partial\phi}{\partial\eta}\Big)_{(i,n)}=\frac{\phi_{i+1}^n-\phi_i^n}{\Delta\eta},$$

$$\Big(\frac{\partial^2\phi}{\partial\eta^2}\Big)_{(i,n)}=\frac{\phi_{i+1}^n-2\phi_i^n+\phi_{i-1}^n}{(\Delta\eta)^2},$$

$$\Big(\frac{\partial\phi}{\partial\tau}\Big)_{(i,n)}=\frac{\phi_i^{n+1}-\phi_i^n}{\Delta\tau},$$

where the superscripts 'n' and '$n+1$' denote the solution at the nth and $(n+1)$th time levels. Also, i, $i-1$, and $i+1$ represent current, previous, and next locations of the solution. Inserting all these approximations into Eqs. (16), (17), and (18), we get:

$$\frac{F_i^{n+1}-F_i^n}{\Delta\tau}-\frac{F_{i+1}^n-2F_i^n+F_{i-1}^n}{(\Delta\eta)^2}$$
$$-f_i^n\frac{F_{i+1}^n-F_i^n}{\Delta\eta}+(F^n)^2$$
$$+\Big(M+\frac{1}{\mathrm{Da}}\Big)\frac{F_{i+1}^n-F_i^n}{\Delta\eta}-\mathrm{Gr}\theta_i^n=0,$$

$$\mathrm{Pr}\frac{\theta_i^{n+1}-\theta_i^n}{\Delta\tau}+\mathrm{Pr}\theta_i^nF_i^n-\mathrm{Pr}f_i^n\Big(\frac{\theta_{i+1}^n-\theta_i^n}{\Delta\eta}\Big)\ notag$$
$$-(1+Nr)\frac{\theta_{i+1}^n-2\theta_i^n+\theta_{i-1}^n}{(\Delta\eta)^2}$$
$$-\mathrm{EcPr}\Big(\frac{F_{i+1}^n-F_i^n}{\Delta\eta}\Big)^2$$
$$-\mathrm{EcPr}\Big(M+\frac{1}{\mathrm{Da}}\Big)(F_i^n)^2-\mathrm{Pr}S\theta_i^n$$
$$-\mathrm{Pr}Nb\Big(\frac{\theta_{i+1}^n-\theta_i^n}{\Delta\eta}\Big)\Big(\frac{\phi_{i+1}^n-\phi_i^n}{\Delta\eta}\Big)$$
$$-Nt\mathrm{Pr}\Big(\frac{\theta_{i+1}^n-\theta_i^n}{\Delta\eta}\Big)^2=0,$$

$$\mathrm{Le}\frac{\phi_i^{n+1}-\phi_i^n}{\Delta\tau}+\mathrm{Le}\Big(\phi_i^nF_i^n-f_i^n\frac{\phi_{i+1}^n-\phi_i^n}{\Delta\eta}\Big)$$
$$-\frac{\phi_{i+1}^n-2\phi_i^n+\phi_{i-1}^n}{(\Delta\eta)^2}$$
$$-\frac{Nt}{Nb}\frac{\theta_{i+1}^n-2\theta_i^n+\theta_{i-1}^n}{(\Delta\eta)^2}=0.$$

The initial and boundary conditions involved are:

$$F_i^0=0, \quad f_i^0=0, \quad \theta_i^0=0, \quad \phi_i^0=0,$$

$$F_0^n=1+\lambda\frac{F_1^n-F_0^n}{(\Delta\eta)}, \quad f_0^n=0, \quad \theta_0^n=1,$$

$$\phi_0^n=1, \quad F_{\eta_\infty}^n=0, \quad \theta_{\eta_\infty}^n=0, \quad \phi_{\eta_\infty}^n=0.$$

The discretization of the skin friction coefficient, the local Nusselt number, and the local Sherwood number for the unsteady flow is performed through:

Skin friction coefficient

$$C_f=\frac{\tau_w}{\rho u_w^2}, \quad \text{where} \quad u_w=\frac{\partial u}{\partial y},$$

$$\sqrt{\mathrm{Re}_x}C_f = \frac{\partial^2 f(0,\tau)}{\partial \eta^2} = \frac{\partial F(0,\tau)}{\partial \eta},$$

$$\sqrt{\mathrm{Re}_x}C_f = \frac{F_1^n - F_0^n}{(\Delta\eta)}.$$

Local Nusselt number:

$$\mathrm{Nu}_x = \frac{xq_w}{k(T_w - T_\infty)}, \quad \text{where :}$$

$$q_w = -k\Big(1 + \frac{16\sigma^* T_\infty^3}{3k^* k}\Big)\frac{\partial T}{\partial y},$$

$$\frac{\mathrm{Nu}_x}{\sqrt{\mathrm{Re}_x}} = -(1+Nr)\frac{\partial \theta(0,\tau)}{\partial \eta},$$

$$\frac{\mathrm{Nu}_x}{\sqrt{\mathrm{Re}_x}} = -(1+Nr)\frac{\theta_1^n - \theta_0^n}{\Delta\eta}.$$

Local Sherwood number:

$$\mathrm{Sh}_x = \frac{xj_w}{k(C_w - C_\infty)}, \quad \text{where :}$$

$$j_w = -D\frac{\partial C}{\partial y}|_{y=0},$$

$$\frac{\mathrm{Sh}_x}{\sqrt{\mathrm{Re}_x}} = -\frac{\partial \phi(0,\tau)}{\partial \eta}$$

$$\frac{\mathrm{Sh}_x}{\sqrt{\mathrm{Re}_x}} = -\frac{\phi_1^n - \phi_0^n}{\Delta\eta}.$$

3.1.1. Grid convergence analysis of unsteady flow

Because of the lack of data on unsteady flow for comparison, we tried to evaluate the convergence of our results by the grid convergence check of the underlying FDM. In Figures 3–6, we display grid convergence for velocity, temperature gradient, concentration gradient, and the skin friction coefficient. It is notable that almost 150 nodal points are enough to get convergent results.

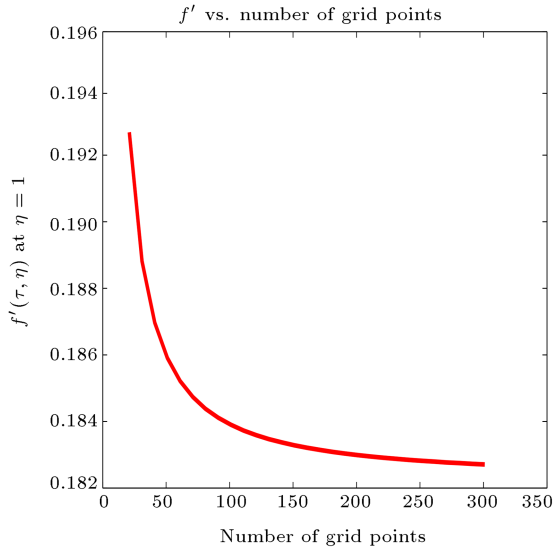

Figure 3. Grid convergence for velocity.

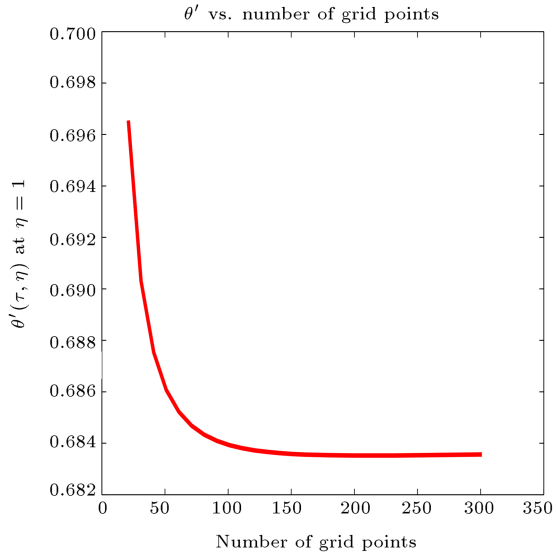

Figure 4. Grid convergence for temperature gradient.

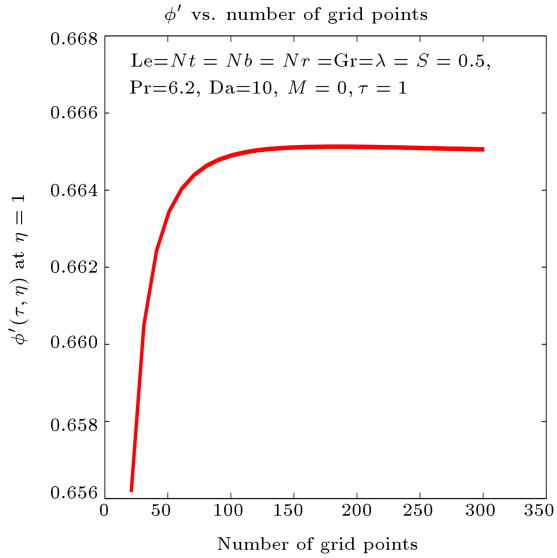

Figure 5. Grid convergence for concentration gradient.

4. Steady flow analysis

For the steady flow, the governing problem given in Eqs. (16)–(18) reduces into:

$$f''' + ff'' - (f')^2 - \Big(M + \frac{1}{\mathrm{Da}}\Big)f' + \mathrm{Gr}\theta = 0, \quad (22)$$

$$\mathrm{Pr}[(\theta f' - f\theta') - \mathrm{Ec}(f'')^2 - \mathrm{Ec}\Big(M + \frac{1}{\mathrm{Da}}\Big)(f')^2 - S\theta - Nb\theta'\phi' - Nt(\theta')^2] - (1+Nr)\theta'' = 0, \quad (23)$$

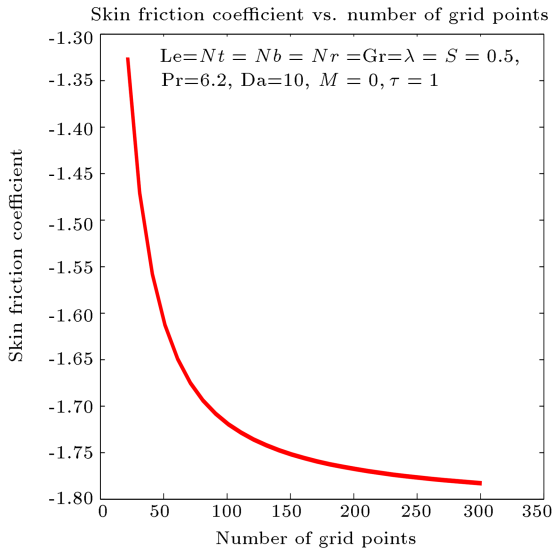

Figure 6. Grid convergence for the skin friction coefficient.

$$\mathrm{Le}(\phi f^{'} - f\phi^{'}) - \phi^{''} - \frac{Nt}{Nb}\theta^{''} = 0, \tag{24}$$

with:

$$f^{'}(0)=1+\lambda f^{''}(0), \quad f(0)=0, \quad \theta(0)=1, \quad \phi(0)=1, \tag{25}$$

$$f^{'}(\infty) = 0, \quad \theta(\infty) = 0, \quad \phi(\infty) = 0. \tag{26}$$

These equations have been solved by the built-in solver *bvp4c* in MATLAB.

4.1. Numerical procedure

To implement *bvp4c* for computing solutions to Eqs. (22)–(26), we first define $y_1 = f$, $y_2 = f^{'}$, $y_3 = f^{''}$, $y_4 = \theta$, $y_5 = \theta'$, $y_6 = \phi$, and $y_7 = \phi'$. Then the first-order system is written as:

$$y_1^{'} = y_2, \quad y_2^{'} = y_3,$$

$$y_3^{'} = -y_1 y_3 + y_2^2 + \left(M + \frac{1}{\mathrm{Da}}\right) y_2 - Gr y_4,$$

$$y_4^{'} = y_5,$$

$$y_5^{'} = \frac{\mathrm{Pr}}{1+Nr}\left[(y_4 y_2 - y_1 y_5) - \mathrm{Ec}\, y_3^2 - \mathrm{Ec}\left(M + \frac{1}{\mathrm{Da}}\right) y_2^2 - S y_4 - Nb y_5 y_7 - Nt y_5^2\right],$$

$$y_6^{'} = y_7, \quad y_7^{'} = \phi^{''} = \mathrm{Le}(y_6 y_2 - y_1 y_7) - \frac{Nt}{Nb} y_5^{'}. \tag{27}$$

Similarly, the boundary conditions used for implementation in MATLAB are:

$$y_0(2) = 1 + \lambda y_0(3), \quad y_0(1) = 0,$$

$$y_0(4) = 1, \quad y_0(6) = 1, \quad y_{inf}(2) = 0,$$

$$\theta_{inf}(4) = 0, \quad \phi_{inf}(6) = 0. \tag{28}$$

The physical parameters in this study are the skin friction coefficient, the local Nusselt number, and the local Sherwood number, which can readily be obtained from Eqs. (13), (14), and (15), respectively, i.e.:

The skin friction coefficient:

$$\sqrt{\mathrm{Re}_x} C_f = -f^{''}(0),$$

The local Nusselt number:

$$\frac{\mathrm{Nu}_x}{\sqrt{\mathrm{Re}_x}} = -(1+Nr)\theta^{'}(0),$$

The local Sherwood number:

$$\frac{\mathrm{Sh}_x}{\sqrt{\mathrm{Re}_x}} = -\phi^{'}(0).$$

5. Results and discussion

The result in Table 1 show the excellent agreement with the literature for the skin friction coefficient in steady flow. In Table 2, the results for the skin friction coefficient indicate that its value increases with increase in the values of Pr and M. The local Nusselt number surges with the values of Pr, Gr, and Da. The local Sherwood number experiences an upward trend with Gr, Rd, Da, Nb, Ec and Le.

Table 1. Comparing $-f^{''}(0)$ with the results in the literature for steady flow analysis.

M	Mabood and Das [42]	Mabood and Shateyi [43]	Present result (*bvp4c*)
0	1.1000008	1.0000084	1.0000
1	1.4142125	1.41421356	1.4142
5	2.4494897	2.44948974	2.4495
10	3.3166247	3.31662479	3.3166
50	7.1414284	7.14142843	7.1414
100	10.049875	10.0498756	10.0499
500	22.383029	22.3830293	22.3830
1000	31.638584	31.6385840	31.6386

Table 2. Values of $-f''(0)$, $-\theta'(0)$, and $-\phi'(0)$ with different values of Pr, M, Gr, λ, Nr, Da, Ec, Nb, Nt, and Le.

										bvp4c		
Pr	**M**	**Gr**	**λ**	**Nr**	**Da**	**Ec**	***Nb***	***Nt***	Le	$-f''(0)$	$-\theta'(0)$	$-\phi'(0)$
0.72	0.5	0.5	0.1	0.2	0.2	0.2	0.1	0.2	1.5	1.8624	0.2488	0.6630
1										1.8658	0.2912	0.5959
2										1.8746	0.3909	0.4310
0.72	0	0.5	0.1	0.2	0.2	0.2	0.1	0.2	1.5	1.7921	0.2689	0.6642
	0.5									1.8624	0.2488	0.6630
	1									1.9289	0.2340	0.6621
0.72	0.5	0	0.1	0.2	0.2	0.2	0.1	0.2	1.5	2.0063	0.1526	0.5549
		1								1.7252	0.2962	0.7296
		2								1.4600	0.3511	0.8355
0.72	0.5	0.5	0	0.2	0.2	0.2	0.1	0.2	1.5	2.3691	0.2161	0.8459
			0.3							1.3129	0.2645	0.4913
			0.5							1.0167	0.2637	0.4115
0.72	0.5	0.5	0.1	0.4	0.2	0.2	0.1	0.2	1.5	1.8607	0.2263	0.6974
				0.6						1.8594	0.2088	0.7236
				0.8						1.8583	0.1946	0.7442
0.72	0.5	0.5	0.1	0.2	0.5	0.2	0.1	0.2	1.5	1.3564	0.4059	0.6770
					1					1.1191	0.4889	0.6877
					1.5					1.0264	0.5227	0.6924
0.72	0.5	0.5	0.1	0.2	0.2	0	0.1	0.2	1.5	1.8658	0.4114	0.3659
						0.3				1.8607	0.1673	0.8117
						0.5				1.8573	0.0039	1.1093
0.72	0.5	0.5	0.1	0.2	0.2	0.2	0.2	0.2	1.5	1.8621	0.2395	0.7858
							0.5			1.8609	0.2131	0.8603
							0.7			1.8602	0.1969	0.8749
0.72	0.5	0.5	0.1	0.2	0.2	0.2	0.1	0.1	1.5	1.8627	0.2532	0.7738
								0.2		1.8624	0.2488	0.6630
								0.4		1.8620	0.2405	0.4601
0.72	0.5	0.5	0.1	0.2	0.2	0.2	0.2	0.2	0.7	1.8626	0.2536	0.2017
									1	1.8625	0.2510	0.3944
									1.5	1.8624	0.2488	0.6630

In Figures 7 and 8 an upsurge tendency is observed in the velocity profile with the un-steady parameter τ under the influence of thermophoresis and magnetic parameters.

Figures 9 and 10 also illustrate the effects of thermophoresis and magnetic parameters with rising value of the unsteady parameter τ for the temperature profile. In the absence of Nt, the temperature is higher and thermal boundary layer thickness increases. When $Nt = 2$, the temperature is reduced significantly, as indicated in Figure 9, due to the migration of molecules. Figure 10 demonstrates an increase in the temperature near the boundary for $M = 0$ and $M = 1$. When the magnetic parameter is non-zero, velocity is reduced and hence, the temperature rises in the fluid flow.

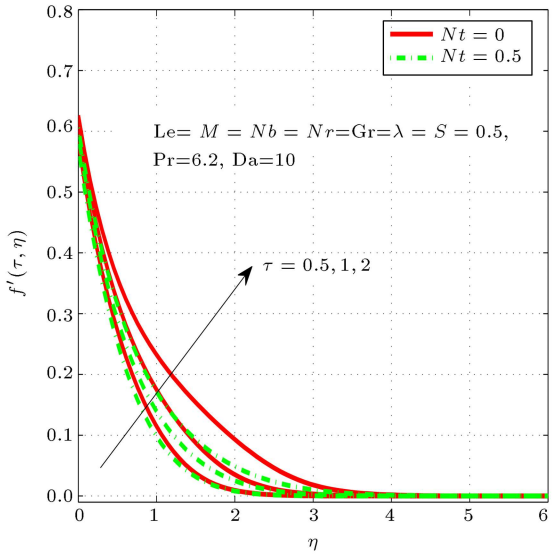

Figure 7. Computational velocity profile against various values of Nt.

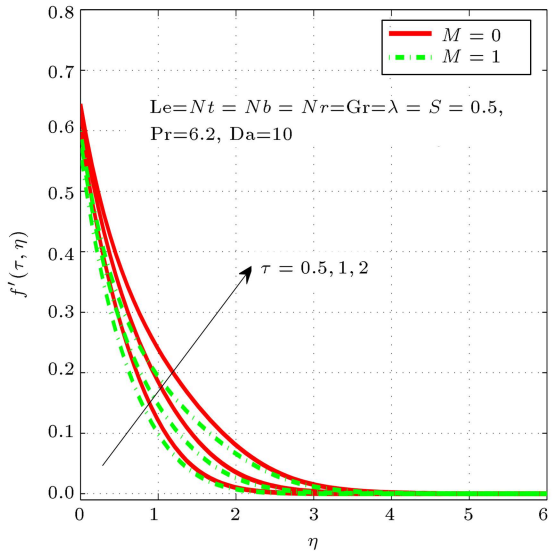

Figure 8. Computational velocity profile against various values of M.

Figure 11 illustrates the effect of Gr on concentration profile with increase in Da. Gr has a huge impact on the concentration profile as observed in the comparison results for Gr = 0 and Gr = 2. We find that the concentration in Figure 12 increases in the presence and absence of M. When $M = 3$, the Lorenz force is stronger, thus reducing the velocity and enlarging the concentration.

Finally, in Figure 13, it is depicted that by neglecting buoyancy and with stronger permeability, Da, temperature is higher near the surface. However, when the buoyancy effect is included in the system, with Gr = 2, the temperature is lower since the variation in permeability obstructs the heat flow.

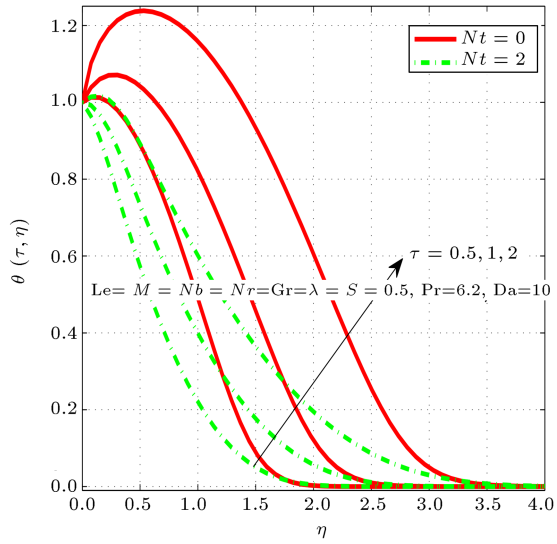

Figure 9. Computational temperature against various values of Nt.

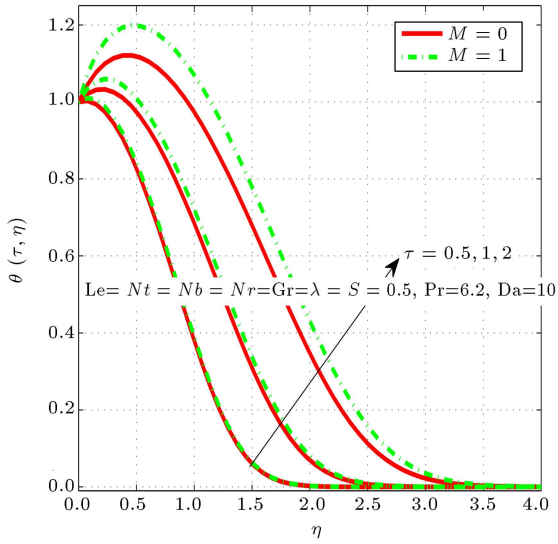

Figure 10. Computational temperature against various values of M.

6. Conclusions

This study presented a numerical solution for unsteady and steady magnetohydrodynamic (MHD) nanofluid flow above a slippery stretching sheet immersed in a porous medium. The key findings are:

- In the steady flow, the skin friction coefficient rises with Pr and M, while it declines with all other parameters. The local Nusselt number experiences an increasing trend with Pr, Gr, and Da. The local Sherwood number rises with Gr, Rd, Da, Ec, Nb, and Le;
- In the unsteady case, the convergence of the numerical discourse was observed in the graphs and

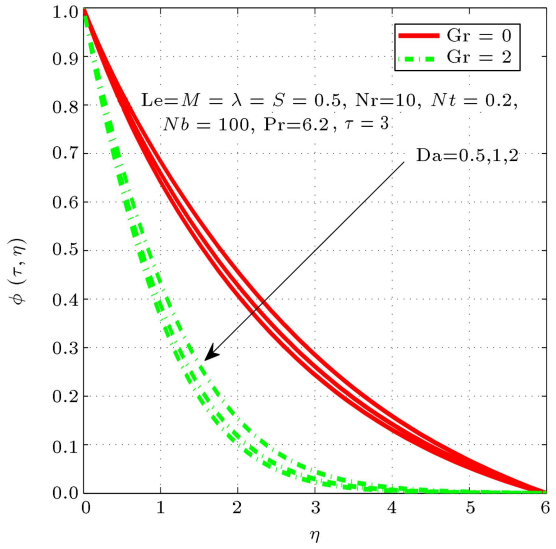

Figure 11. Computational concentration profile against variations of different parameters.

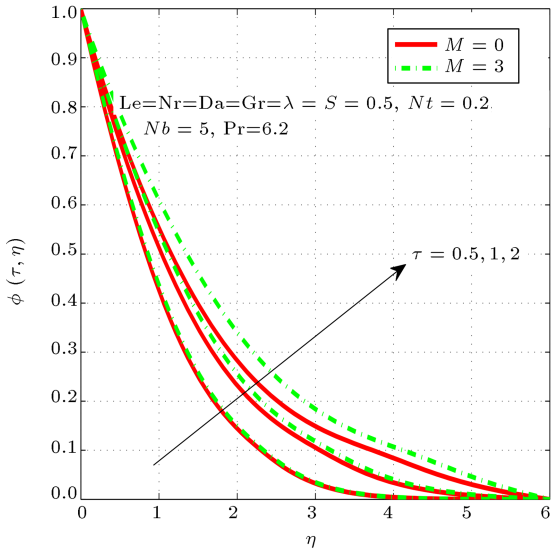

Figure 12. Computational concentration profile against various values of different parameters .

it was demonstrated that approximately 150 grid points sufficed for the numerical solution;

- In the unsteady case, with an increase in nondimensional time, the thermophoresis and magnetic parameters had the same effect, i.e. the momentum boundary layer thickness increase;
- For unsteady flow, the nanofluid concentration profile is strongly dependent on the Grashof number and it decreases with increasing Da;
- In the unsteady case, the required stability of concentration profile is met possible by fine tuning of the values of the thermophoresis and Brownian motion parameters;
- The effect of unsteadiness was also visible in temperature profile. A significant increase in thermal boundary layer was found with Nt and M.

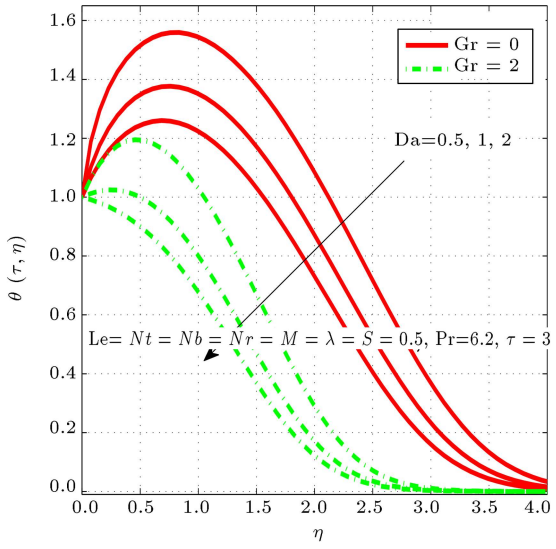

Figure 13. Computational temperature against various values of Gr.

Nomenclature

(u, v)	Velocity components
μ	Coefficient of viscosity
ρ	Density of fluid
σ	Electrical conductivity of fluid
T	Fluid temperature
K	Porous medium permeability
β	Thermal expansion coefficient
k	Thermal conductivity
C_p	Specific heat capacity
q_r	Radiative heat flux
Q	Heat source coefficient
C	Concentration
τ	Time
$(\rho C)_p$	Heat capacities of nanofluid
$(\rho C)_f$	Heat capacities of base fluid
C_p	Specific heat at constant pressure
D_B	Brownian coefficient
D_T	Thermophoretic diffusion coefficient
T_∞	Ambient fluid temperature
C_∞	Ambient fluid concentration
Pr	Prandtl number
Gr	Grashof number
Le	Lewis number
Nt	Thermophoresis number
Nb	Brownian motion parameter

λ	Slip parameter
S	Heat source parameter
Nr	Thermal radiation parameter
Ec	Eckert number
Da	Darcy number
M	Magnetic parameter

References

1. Khan, Z., Rasheed, H.U., Alkanhal, T.A., Ullah, M., Khan, I., and Tlili, I. "Effect of magnetic field and heat source on upper-convected-Maxwell fluid in a porous channel", *Open Physics*, **16**, pp. 917–928 (2018).
2. Kumar, P.S., Gireesha, B.J., Mahanthesh, B., and Chamkha, A.J. "Thermal analysis of nanofluid flow containing gyrotactic microorganisms in bioconvection and second-order slip with convective condition", *J. Therm. Anal.*, **136**, pp. 1947–1957 (2019).
3. Choi, S.U. and Eastman, J.A. "Enhancing thermal conductivity of fluids with nanoparticles", No. ANL/MSD/CP-84938; CONF-951135-29; Argonne National Lab., IL (United States) (1995).
4. Philip, J., Shima, P.D., and Raj, B. "Nanofluid with tunable thermal properties", *Appl. Phys. Lett.*, **92**, p. 043108 (2008).
5. Kao, M.J., Lo, C.H., Tsung, T.T., Wu, Y.Y., Jwo, C.S., and Lin, H.M. "Copper-oxide brake nanofluid manufactured using arc-submerged nanoparticle synthesis system", *J. Alloys Compd.*, **434**, pp. 672–674 (2007).
6. Yu, W. and Xie, H. "A review on nanofluids: preparation, stability mechanisms, and applications", *J. Nanomater.*, **2012**, pp. 1–17 (2012).
7. Mahian, O., Kianifar, A., Kalogirou, S.A., Pop, I., and Wongwises, S. "A review of the applications of nanofluids in solar energy", *Int. J. Heat Mass Transfer*, **57**, pp. 582–594 (2013).
8. Angayarkanni, S.A. and Philip, J. "Review on thermal properties of nanofluids: Recent developments", *Advances in Colloid and Interface Science*, **225**, pp. 146–176 (2015).
9. Hung Thang, B., Le Quang, D., Manh Hong, N., Khoi, P.H., and Minh, P.N. "Application of multiwalled carbon nanotube nanofluid for 450 W LED flood light", *J. Nanomater.,* **2014**, pp. 1–6 (2014).
10. Mahendran, V. and Philip, J. "Naked eye visualization of defects in ferromagnetic materials and components", *NDT & E. Int*, **60**, pp. 100–109 (2013).
11. Liakos, I., Grumezescu, A.M., and Holban, A.M. "Magnetite nanostructures as novel strategies for anti-infectious therapy", *Molecules*, **19**, pp. 12710–12726 (2014).
12. Buongiorno, J. "Convective transport in nanofluids", *J. Heat Transfer*, **128**, pp. 240–250 (2006).
13. Das, K., Duari, P.R., and Kundu, P.K. "Nanofluid flow over an unsteady stretching surface in presence of thermal radiation", *Alex. Eng. J.*, **53**, pp. 737–745 (2014).
14. Atif, S.M., Hussain, S., and Sagheer, M. "Heat and mass transfer analysis of time-dependent tangent hyperbolic nanofluid flow past a wedge", *Physics Letters A*, **383**(11), pp. 1187–1198 (2019).
15. Azam, M., Shakoor, A., Rasool, H.F., and Khan, M. "Numerical simulation for solar energy aspects on unsteady convective flow of MHD cross nanofluid: A revised approach", *Int. J. Heat Mass Transf.*, **131**, pp. 495–505 (2019).
16. Khan, M., Huda, N.U., and Hamid, A. "Non-linear radiative heat transfer analysis during the flow of Carreau nanofluid due to wedge-geometry: A revised model", *Int. J. Heat Mass Transf.*, **131**, pp. 1022–1031 (2019).
17. Hayat, T., Aziz, A., Muhammad, T., and Alsaedi, A. "Numerical simulation for three-dimensional flow of Carreau nanofluid over a nonlinear stretching surface with convective heat and mass conditions", *J. Braz. Soc. Mech. Sci.*, **41**, pp. 41–55 (2019).
18. Ghadikolaei, S.S., Hosseinzadeh, K., Ganji, D.D., and Hatami, M. "$Fe_3O_4(CH_2OH)_2$ nanofluid analysis in a porous medium under MHD radiative boundary layer and dusty fluid", *J. Mol. Liq*, **258**, pp. 172–185 (2018).
19. Rossow, V.J. "On flow of electrically conducting fluids over a flat plate in the presence of a transverse magnetic field", NASA, Report No. 1358, 489 (1958).
20. Raptis, A., Perdikis, C., and Takhar, H.S. "Effect of thermal radiation on MHD flow", *Appl. Math. Comput.*, **153**, pp. 645–649 (2004).
21. Fang, T., Zhang, J., and Yao, S. "Slip MHD viscous flow over a stretching sheet. An exact solution", *Commun. Nonlinear Sci. Numer. Simul.*, **14**, pp. 3731–3737 (2009).
22. Makinde, O.D., Mabood, F., Khan, W.A., and Tshehla, M.S. "MHD flow of a variable viscosity nanofluid over a radially stretching convective surface with radiative heat", *J. Mol. Liq*, **219**, pp. 624–630 (2016).
23. Nield, D.A. and Kuznetsov, A.V. "The Cheng-Minkowycz problem for natural convective boundary-layer flow in a porous medium saturated by a nanofluid", *Int. J. Heat Mass Transfer.*, **52**, pp. 5792–5795 (2009).
24. Hayat, T., Saif, R.S., Ellahi, R., Muhammad, T., and Alsaedi, A. "Simultaneous effects of melting heat and internal heat generation in stagnation point flow of Jeffrey fluid towards a nonlinear stretching surface with variable thickness", *Int. J. Therm. Sci.,* **132**, pp. 344–354 (2018).

25. Makinde, O.D., Khan, Z.H., Ahmad, R., and Khan, W.A. "Numerical study of unsteady hydromagnetic radiating fluid flow past a slippery stretching sheet embedded in a porous medium", *Phys. Fluids*, **30**, p. 083601 (2018).

26. Malik, M.Y., Naseer, M., Nadeem, S., and Rehman, A. "The boundary layer flow of Casson nanofluid over a vertical exponentially stretching cylinder", *Appl. Nanosci.*, **4**, pp. 869–873 (2014).

27. Jusoh, R., Nazar, R., and Pop, I. "Flow and heat transfer of magnetohydrodynamic three-dimensional Maxwell nanofluid over a permeable stretching/shrinking surface with convective boundary conditions", *J. Comput. Theor. Nanosci.*, **14**, pp. 1644–1652 (2017).

28. Bhaskar Reddy, N., Poornima, T., and Sreenivasulu, P. "Influence of variable thermal conductivity on MHD boundary layer slip flow of ethylene-glycol based Cu nanofluids over a stretching sheet with convective boundary condition", *Int. J. of Eng. Math.*, **2014**, pp. 1–10 (2014).

29. Hakeem, A.A., Kalaivanan, R., Ganesh, N.V., and Ganga, B. "Effect of partial slip on hydromagnetic flow over a porous stretching sheet with non-uniform heat source/sink, thermal radiation and wall mass transfer", *Eng. Phys. and Math.*, **5**, pp. 913–922 (2014).

30. Cortell, R. "Flow and heat transfer of a fluid through a porous medium over a stretching surface with internal heat generation/absorption andsuction/blowing", *Fluid Dyn. Res.*, **37**, p. 231 (2005).

31. Cai, W., Su, N., and Liu, X. "Unsteady convection flow and heat transfer over a vertical stretching surface", *PLoS One*, **9**, p. 111 (2014).

32. Wang, C.Y. "Flow due to stretching boundary with partial slip- an exact solution of the navier-stokes equation", *Chem. Eng. Sci.*, **57**, pp. 3745–3747 (2002).

33. Noghrehabadi, A., Pourrajab, R., and Ghalambaz, M. "Effect of partial slip boundary condition on the flow and heat transfer of nanofluids past stretching sheet prescribed constant wall temperature", *Int. J. Therm. Sci.*, **54**, pp. 253–261 (2012).

34. Ariel, P.D., Hayat, T., and Asghar, S. "The flow of an elastico-viscous fluid past a stretching sheet with partial slip", *Acta Mechanica*, **187**(1–4), pp. 29–35 (2006).

35. Fatunmbi, E.O. and Fenuga, O.J. "Heat and mass transfer of a chemically reacting MHD micropolar fluid flow over an exponentially stretching sheet with slip effects", *Physical Science International Journal*, **18**(3), pp. 1–15 (2018).

36. Khan, N.S., Zuhra, S., Shah, Z., Bonyah, E., Khan, W., and Islam, S. "Slip flow of Eyring-Powell nanoliquid film containing graphene nanoparticles", *AIP Advances*, **8**(11), p. 115302 (2018).

37. LeVeque, R.J., *Finite Difference Methods for Ordinary and Partial Differential Equations: Steady-State and Time-Dependent Problems*, Siam (2007).

38. LeVeque, R.J., *Finite Volume Methods for Hyperbolic Problems*, Cambridge University Press (2002).

39. Sheikholeslami, M. "CuO-water nanofluid flow due to magnetic field inside a porous media considering Brownian motion", *J. Mol. Liq.*, **249**, pp. 921–929 (2018).

40. Reza-E-Rabbi, Sk, Arifuzzaman, S.M., Tanmoy Sarkar, Md Shakhaoath Khan, and Sarder Firoz Ahmmed. "Explicit finite difference analysis of an unsteady MHD flow of a chemically reacting Casson fluid past a stretching sheet with Brownian motion and thermophoresis effects", *Journal of King Saud University-Science*, **32**(1), pp. 690-701 (2020).

41. Shampine, L.F., Kierzenka, J., and Reichelt, M.W. "Solving boundary value problems for ordinary differential equations in MATLAB with bvp4c", *Tutorial Notes*, pp. 1–17 (2000).

42. Mabood, F. and Das, K. "Melting heat transfer on hydromagnetic flow of a nanofluid over a stretching sheet with radiation and second-order slip", *Eur. Phys. J. Pl.*, **131**(1), pp. 1–12 (2016).

43. Mabood, F. and Shateyi, S. "Multiple slip effects on MHD unsteady flow heat and mass transfer impinging on permeable stretching sheet with radiation", *Model. Sim. Engi.*, **2019** (2019).

Biographies

M. Asif Farooq received his MSc and MPhil degrees from Quaid-i-Azam University, Islamabad, Pakistan, in 2005 and 2007, respectively. He obtained PhD degree in Computational Fluid Dynamics from the Norwegian University of Science and Technology, Trondheim, Norway. He has been serving at National University of Sciences and Technology (NUST), Islamabad, Pakistan, since 2012. His research interests include computational fluid dynamics.

A. Salahuddin received BSc degree from Fatima Jinnah Women University, Rawalpindi, Pakistan, in 2017 and MSs degree from the National University of Sciences and Technology, Islamabad, Pakistan, in 2019. Her research interests include fluid mechanics and numerical analysis of partial differential equations.

M. Razzaq obtained his PhD in Applied Mathematics from the Technical University of Dortmund, Germany, in 2011. He has been serving at Lahore University of Management Sciences, Lahore, Pakistan, since 2017. His research primarily bridges the area of Computational Fluid Dynamics (CFD) and Computational Solid Mechanics (CSM), namely Fluid-Structure Inter-

action (FSI). His research interests include numerical analysis and scientific computing, finite element methods, and fluid-structure interaction.

S. Hussain obtained MSc degree in Applied Mathematics from Bahuddin Zakaria University, Multan, Pakistan, in 2008. Then, he proceeded to obtain another MSc degree from Sussex University, UK, in 2017. His research interests include computational techniques for partial differential equations.

Asif Mushtaq received his PhD in Applied Mathematics from the Norwegian University of Science and Technology, Trondheim, Norway, in 2014. He has been working as an Associate Professor of Mathematics at Nord University Bod campus since 2016. His research interests include numerical analysis, statistical analysis, and mathematics education.